Scientific Research Publishing

Open Journal of Geology, 2025, 15(12), 972-985
https://www.scirp.org/journal/ojg
ISSN Online: 2161-7589
ISSN Print: 2161-7570

Cinder Cones Geomorphometric Dating in the Camargo Volcanic Field, Chihuahua, Mexico

Vanessa Veronica Espejel-Garcia[1*], Alejandro Villalobos-Aragon[1], Daphne Espejel-Garcia[1], Martha Iveth Gallegos-Aragon[2], Marina Esmeralda Chavez-Armendariz[2]

[1]School of Engineering, Autonomous University of Chihuahua, Chihuahua, Mexico
[2]Independent Geology Consultants, Chihuahua, Mexico
Email: *vespejel@uach.mx

How to cite this paper: Espejel-Garcia, V.V., Villalobos-Aragon, A., Espejel-Garcia, D., Gallegos-Aragon, M.I. and Chavez-Armendariz, M.E. (2025) Cinder Cones Geomorphometric Dating in the Camargo Volcanic Field, Chihuahua, Mexico. *Open Journal of Geology*, **15**, 972-985.
https://doi.org/10.4236/ojg.2025.1512050

Received: November 9, 2025
Accepted: December 8, 2025
Published: December 11, 2025

Abstract

The Camargo Volcanic Field (CVF), located in the southeastern portion of the Mexican state of Chihuahua, is part of the Basin & Range province. With a surface of nearly 3000 km^2 and composed of approximately 300 cinder cones, it is considered the largest alkaline mafic volcanic field in northern Mexico. Radiometric analyses have yielded absolute ages ranging from 4 to 0.09 Ma. Cinder cones are landforms that do not show significant variations in composition or shape, leading to constant erosion. Specifically, the relationship between their slope and age has been analyzed in numerous studies, showing that slopes decrease with age; this can then be used as an indicator of the relative age of the cones. This study applies an equation from Miller (2006), which correlates radiometric ages with slope angles from other arid-region cinder cones. Using this method, an exponential trend equation was published in previous work, based on data from cones dated using absolute dating methods and measured using remote sensing imagery. This work presents a geomorphometric study in which slopes and the distribution of 51 cinder cones were measured and analyzed. Digital elevation models, topographic maps, Google Earth, and drone images were processed to measure the cinder cones. Results showed slopes ranging from 3˚ to 13˚, with ages ranging from 226,671 to 99,408 years. The oldest cones are located within the SW portion of CVF, while the youngest cones are found in its north and NE portions. The data obtained were consistent with previous studies; however, it is important to note that the parameters used vary with image resolution. It was concluded that drone images are more accurate for geomorphometric age calculations because they have higher spatial resolution, yielding more precise measurements. Geomorphometric dating is suggested as a preliminary tool in volcanic field studies, but it is always advised to apply radiometric dating to determine the volcanic history of an area.

Keywords

Camargo Volcanic Field, Cinder Cones, Geomorphometric Dating, Image Processing, Volcanic Geomorphology

1. Introduction

Determining the age of rocks and/or minerals provides crucial insights into Earth's history, helping to reconstruct the sequence of geological, geochemical, and tectonic events. Over time, the most widely applied dating techniques are the relative and the radiometric methods, each providing reliable rock ages [1] [2].

Relative dating establishes the chronological order of geological events based on stratigraphic principles and the continuity of the geological record, using stratigraphic relationships and fossil correlations, but does not assign numerical ages [3]. Radiometric dating determines absolute ages in years based on isotopic decay, allowing high precision in dating igneous and metamorphic rocks [2]. Among the radiometric methods, the most used are uranium-lead (U-Pb), potassium-argon (K-Ar), and rubidium-strontium (Rb-Sr) [2] [4]. The advances in analytical instruments have enhanced the accuracy of dating.

There is a third method, used only for certain cases, known as the geomorphometric dating method, which involves quantitative/physical analysis of geological structures or landform morphology, providing temporal information where isotopic or stratigraphic data are limited [5]. These methods develop an integrating approach to reconstructing the geochronology of Earth's crust.

The geomorphometric dating method leverages climatic conditions and geological formations. For example, dating cinder cones is only useful in arid climates and in formations younger than 1 Ma [6].

Geomorphometric dating studies primarily include volcanic fields located in arid zones, among which are the El Potrillo Volcanic Field in New Mexico, USA [7], the Camargo Volcanic Field in Chihuahua, Mexico [8]-[10], and the Lunar Crater Volcanic Field in Nye County, Nevada, USA [11], among others. A brief overview of each is presented in **Table 1**.

In the Camargo Volcanic Field (CVF), the acquisition of isotopic ages is constrained by several factors that justify the use of geomorphometric dating as a complementary tool. Since most of this vast surface is privately owned, access to the sampling sites is limited and can even be dangerous. Additionally, the high cost of radiometric analysis has resulted in a sparse and uneven chronological dataset for the CVF; only one work in the 2000s published absolute ages [12]. These constraints hinder the development of a consistent and detailed geochronological record of eruptions within the CVF. Thus, geomorphometric dating provides a feasible, quick, and low-cost alternative, enabling the estimation of relative or approximate ages when absolute dating is insufficient and the development of a temporal framework for the CVF volcanic evolution.

Table 1. Previous work on cinder cone analyses.

Authors	Published paper	Methodology	Findings
Scott (1971)	Geology of the Lunar Crater Volcanic Field, Nye County, Nevada.	Morphological changes in cinder cones, degree of weathering, and basalt flow superposition were analyzed to determine cone heights, base radius, and slope angles.	Measured cinder cones were classified into 3 groups based on relative age: older, intermediate, and younger.
Porter (1972)	Distribution morphology, and size frequency of cinder cones on Mauna Kea Volcano, Hawaii.	Geomorphological parameters, including crater width-depth, cone height, basal cone width, and maximum slope angle, were measured in 3 symmetrical rupture zones on Mauna Kea volcano in Hawaii.	The cones showed little variation in slope angles (20˚- 27˚). Basal width and cone height were used to classify cones by size.
Bloomfield (1975)	A late-Quaternary monogenetic volcano field in central Mexico.	Non-quantifiable geomorphometric characteristics were considered (erosion status of the upper flanks, base of the cones, condition of the crater rim, and infilling).	The study analyzed 41 cinder cones and lava flows, yielding relative ages of 8,390 ±100 to 40,000 years, based on geomorphological parameters.
Wood (1980)	Morphometric analysis of cinder cones degradation.	Geometric measurements from cinder cones with favorable shapes were obtained. They were related to degradation rates. These rates often vary enormously, so climate is an important factor to consider.	Morphological studies of volcanoes were reviewed by observing certain structures on the surface of the moon, Mars and Venus, since much of a volcano's history can be found in its shape and structure.
Luhr & Carmichael (1981)	The Colima Volcanic Complex, Mexico: Part II. Late-Quaternary cinder cones.	The relative age of 7 cones was calculated from their slope angles, using a constant previously used by Scott and Trask (1971).	The cinder cones' slopes decreased by 11˚ every 20,000 years.
Noyola (1995)	Comparative study of the geology and morphology of some cinder cones in the volcanic fields of Camargo, Chihuahua, and San Quintin, Baja California.	Due to the large Camargo field size, only 11 cones were examined (considered as representative). The cones in the San Quintin field are taller, steeper, and better preserved.	The cones were classified as young and intermediate in the northeastern part of the volcanic fields and mature in the southwestern parts.
Miller (2006)	A morphologic analysis of Quaternary cinder cones, Potrillo Volcanic Field, New Mexico.	Cinder cone ages were calculated from morphological measurements and compared with radiometric ages of the Capulin volcano in the area.	The distribution of slope angles resulted in 3 age groups: old, intermediate, and young. The results were compared with an exponential trend line fitted to radiometric ages of other cinder cones, establishing a relationship between age and cone slope angle.
Pelletier & Cline (2007)	Nonlinear slope-dependent sediment transport in cinder cone evolution.	A general equation was proposed for working with the evolution of gentle and steep slopes. The variable n changes depending on the speed of the transition between linear and nonlinear slope-dependent processes.	It is established that nonlinear sediment transport models can be validated using cinder cones, which can be dated radiometrically and compared.

Continued

Gilichinsky *et al.* (2010)	Morphometric measurements of cinder cones from digital elevation models of the Tolbachik volcanic field, central Kamchatka.	The morphometric parameters derived from a DEM include the main characteristics that control the rate of degradational evolution of the cone, namely height, width, and slope.	Morphometric values obtained from a DEM are affected by the resolution change, and characteristics of the same cinder cone may vary among DEMs of different resolutions.
Gallegos (2013)	Geomorphometric analysis of Neogene and Quaternary cinder cones in the Camargo Volcanic Field, Chihuahua, Mexico.	17% of the cinder cones in the volcanic field were analyzed using Global Mapper 14 software to process topographic maps and DEMs of the Mexican elevation continuum.	The results showed slopes ranging from 4˚ to 13˚ and ages from 226,267 to 99,274 years, respectively.
Kerexturi *et al.* (2013)	Evaluation of morphometry-based dating of monogenetic volcanoes—a case study from Bandas del Sur, Tenerife (Canary Islands).	Parameters were obtained from digital elevation models, and age estimates were derived from the cone height/width ratio and slope angle; the results were compared with K-Ar ages.	Ages do not match, and the degradation trend and changes over time do not support the previously proposed simple degradation model for monogenetic volcanoes.
Zarazúa-Carbajal and De la Cruz-Reyna (2021)	Digital Elevation Model resolution: Effects on the chronometry-oriented morphological analysis of monogenetic scoria cones in the Sierra Chichinautzin, central Mexico.	Morphometric parameters were measured from TanDEM-X SAR and LIDAR DEMs; ages were calculated. Then, compared to the radiometric reported ages.	The age-relevant morphometric parameters calculated from both different DEMs perform equally well for the morpho-chronological characterization of scoria cones.
Chávez (2021)	Geomorphometric study of two cinder cones to the north of the Camargo Volcanic Field, Chih.	Two of the youngest cinder cones from the Camargo volcanic field were measured using DEMs, Google Earth, and drone images. Geomorphometric ages were calculated.	Drone images are more accurate than any other satellite imagery for calculating geomorphometric ages.

This research compares previously published radiometric ages [12] with geomorphometric ages for the best-preserved cinder cones of the Camargo Volcanic Field (CVF) in Chihuahua, Mexico.

2. Geologic Setting

The study area is in the south-central portion of the state of Chihuahua, in the municipality of Camargo, 57 km east of Camargo city, on the border with the Mexican state of Coahuila, between UTM coordinates 533000E, 3042000N and 598000E, 3097000N (see **Figure 1**).

The region known as the Camargo Volcanic Field (CVF) is composed of flows distributed as large alkaline basalt plateaus containing olivine, clinopyroxene, and kaersutite xenocrysts, as well as lower crustal xenoliths that come from near the Mohorovicic discontinuity boundary (peridotites, granulites, paragneisses, and othogneisses [10] [12] [13].

The formation of the CVF is thought to be strongly related to a still-active normal fault trending NW-SE, with evidence that faulting and volcanism may have been contemporaneous [12] [14]. The CVF lies along the trace of the buried San

Marcos regional fault [12], which formed during the Jurassic and was reactivated in multiple deformation pulses.

Based on its age, the field's formation is attributed to the last reactivation, caused by extensional activity in the Basin and Range Province [15]. The most important structural feature of the CVF is a graben located in the center of the field, which divides it into three volcano-tectonic domains: 1) La Loba in the SW portion of the field; 2) El Venado in the central part, and 3) Las Maravillas in the NE portion of the CVF. Each domain is distinguished from the others by the age of its volcanic activity, the density of cones, and the density of faults [12].

The 51 cinder cones measured were selected for their best-preserved form, and are distributed throughout the three domains, with the majority located within the Las Maravillas domain [12] (see **Figure 1**). The cinder cones selected were chosen based on their conserved circular form. The rest of the cones have horse-shoe shapes or irregular base forms that do not allow for measuring the true base and/or crater diameters, which negatively impact age calculations, since these measurements are important for determining the slope angle.

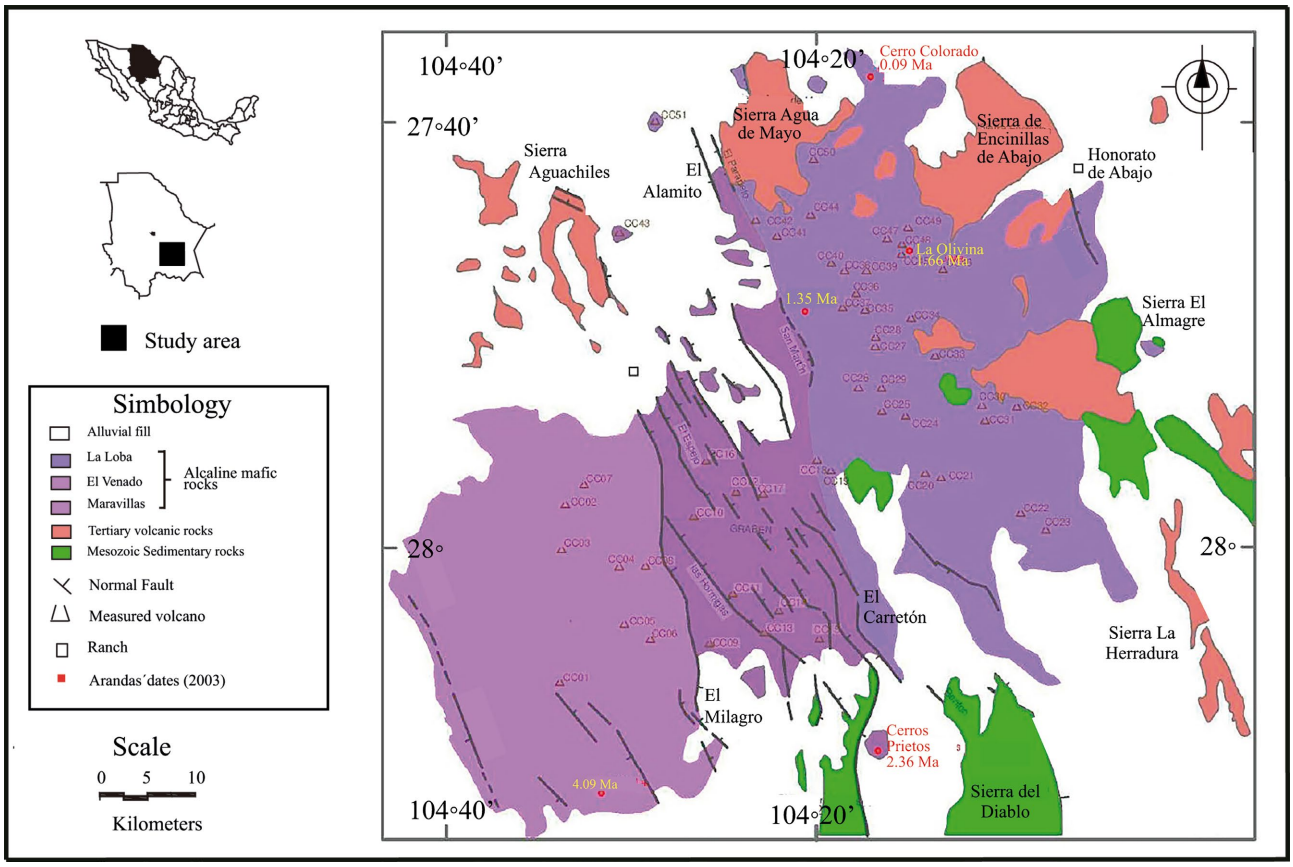

Figure 1. Location and geologic map of the Camargo Volcanic Field (CVF), which shows the 51 cinder cones measured for this research. Adapted from [12] by [9].

3. Methodology

The method used to measure slopes in cinder cones is based on techniques that

analyze volcanic structures using satellite imagery, digital elevation models, Google Earth, and drone imagery. The information processing was performed using Global Mapper 14.

Cinder cones are landforms that do not show significant variations in their composition and shape [16]. This characteristic allows for the establishment of constants in the effects of erosion on them. However, it is important to highlight the role of extrinsic factors that affect or intervene in the erosion process of cones that have a direct influence on the slope angle [16]-[21].

- *Climatic conditions*: The degradation of any type of relief is mostly due to water and wind erosion. In temperate or tropical areas with high annual rainfall, water saturation on slopes often triggers landslides or mass wasting, which act as catalysts for the cones' degradation. The opposite is true in arid zones, where the main erosive agent is wind, and vegetation is absent [16].
- *Cone morphology*: Erosion is more severe in geological structures or landforms with marked relief, while it will be less intense in those structures with bare relief. Young cinder cones will be more affected by erosion than older, semi- or well-degraded cones. As a result, over a given period, the effect of erosion is more evident in young volcanic structures than in semi-eroded ones [16]-[18]. Likewise, cuts in the volcanic structure caused by subsequent lava flows can accelerate erosion.

The choice of slope-angle analysis technique is influenced by the specific environments of the study areas, including location and climatic conditions, as well as the age and characteristics of each cone. Within CVF, a high percentage of volcanic cones are unsuitable for analysis because they are highly eroded, with most exhibiting a horseshoe-shaped crater rim [10]. Based on these criteria, only 51 of the 300 cinder cones [12] have a well-defined shape and were measured.

3.1. Morphometric Measurements

The cinder cones' measurements include the base diameter/radius and the cone's maximum elevation. The Global Mapper 14 software was used to determine these dimensions. The processed images included mostly the Mexican elevation continuum, 1:50,000-scale topographic maps (both provided by the Mexican National Institute of Statistics and Geography, INEGI), and, for two specific cones in the northern part of CVF, Google Earth and drone images (**Figure 2**).

The software allows us to obtain, in addition to a terrain's 3D image, a topographic profile from a user-drawn line (**Figure 3(a)**) and the measurements needed to calculate the slope angle. Data acquisition was carried out as follows:

- *Base diameter/radius:* for each cone, six lines were drawn in different directions to cover most of the circumference of the volcanic structure, and then the average of the 6 lines' lengths corresponds to the base diameter. The base radius measurement is half of the diameter.
- *Cones' maximum elevation (me):* for each of the six lines drawn, the software provided a detailed profile section, obtaining from it the maximum (*me*) and basal elevation (*be*) of each line. The *me* and *be* of each cone were calculated

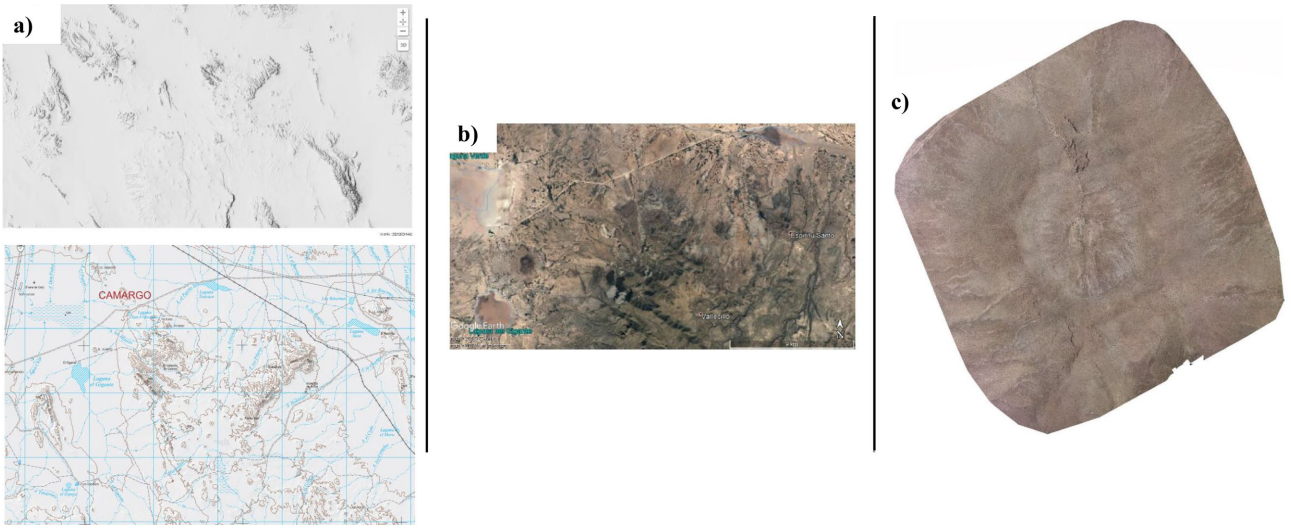

Figure 2. Images used for morphometric measurements: (a) digital elevation models (DEMs) and topographic maps, (b) Google Earth images, and (c) drone images [8].

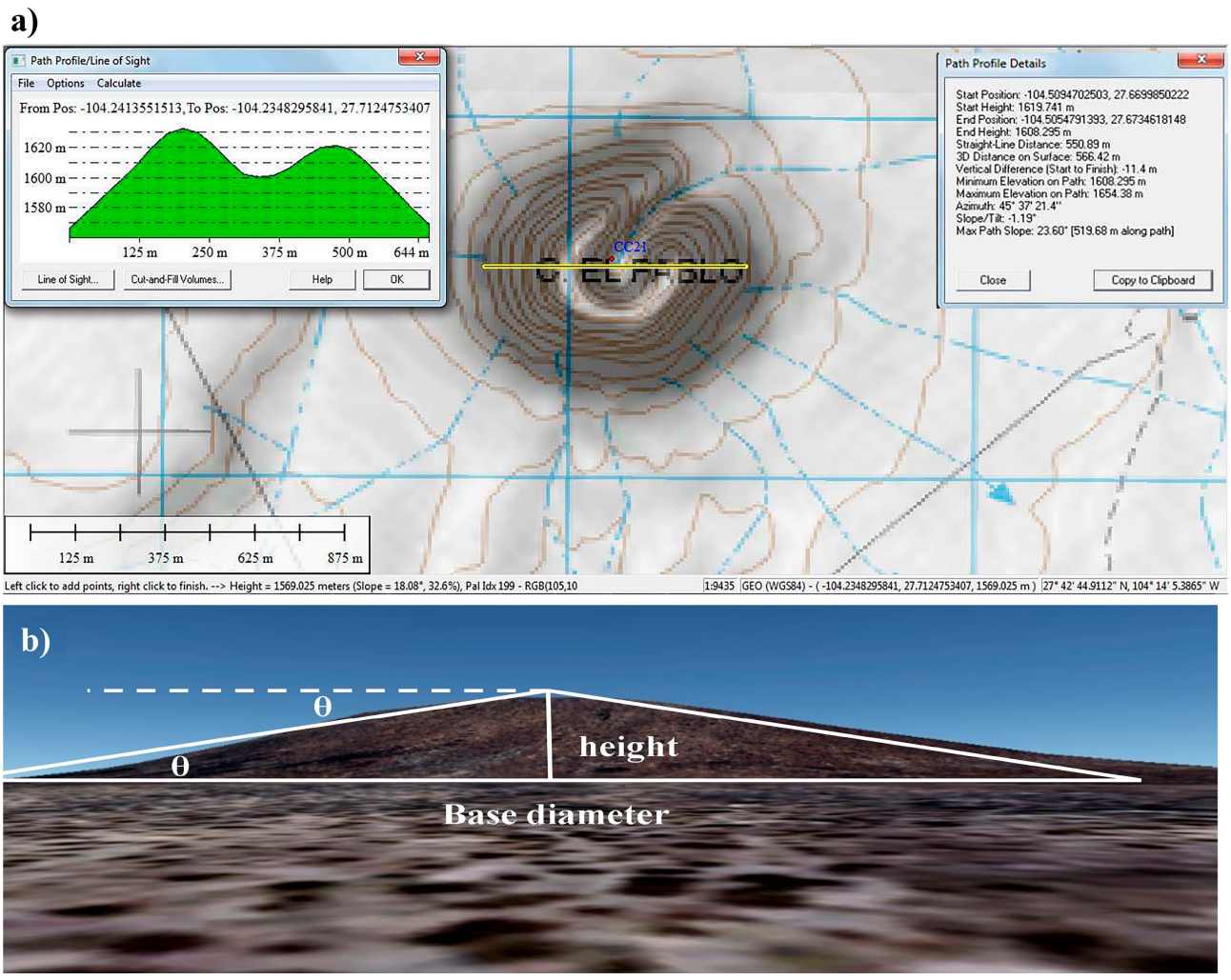

Figure 3. (a) Topographic profile obtained in Global Mapper 14; (b) Measurements in cinder cones for using trigonometry to calculate slope angle [9].

as the average of the six initial heights of the profile. The difference (*me-be*) represents the maximum height (*h*) of the cone.

- *Slope angle:* using the base radius and maximum elevations, the slope angle was calculated using the trigonometric function in Equation (1) (see **Figure 3(b)**).

$$\theta = \tan^{-1}\left(h/\text{average of radii}\right) \tag{1}$$

3.2. Geomorphometric Dating Calculations

Considering previous studies that relate slope angles to the radiometric ages of cinder cones [6] [7] [11], an exponential plot with its corresponding equation was established (**Figure 4**). This equation was proposed by Joseph Miller (2006). In it, he relates data from young cinder cones radiometrically dated, all located in arid zones, to the volcanoes of CVF. The volcanoes considered for this plot were the Paricutin, with an assigned age of 0, since it formed in 1943 [22]; Black Mountain volcanic center from the El Potrillo volcanic field in New Mexico, USA, with an age of 125 ± 11 ka [23]; and Capulin volcano in New Mexico, USA, 56 ± 8 ka [24]; all dated with the $^{40}Ar/^{39}Ar$ radiometric technique. This equation was chosen because the author used cinder cones from similar arid climatic conditions to those in CVF; Black Mountain volcano is about 565 km to the NW of CVF and is part of the same tectonic event, also Chihuahua and New Mexico are within the Chihuahuan desert. The resulting plot shows an exponential trend line with a specific function (Equations (2), (3)), indicating that the degree of erosion reflected in the cones' slope angles increases with time elapsed since the volcanic activity ceased.

$$y = 35e^{-5x}\left(\text{where } R = 1\right) \tag{2}$$

$$y = 3.179e^{-1E-5x}\left(\text{where } R^2 = 0.9999\right) \tag{3}$$

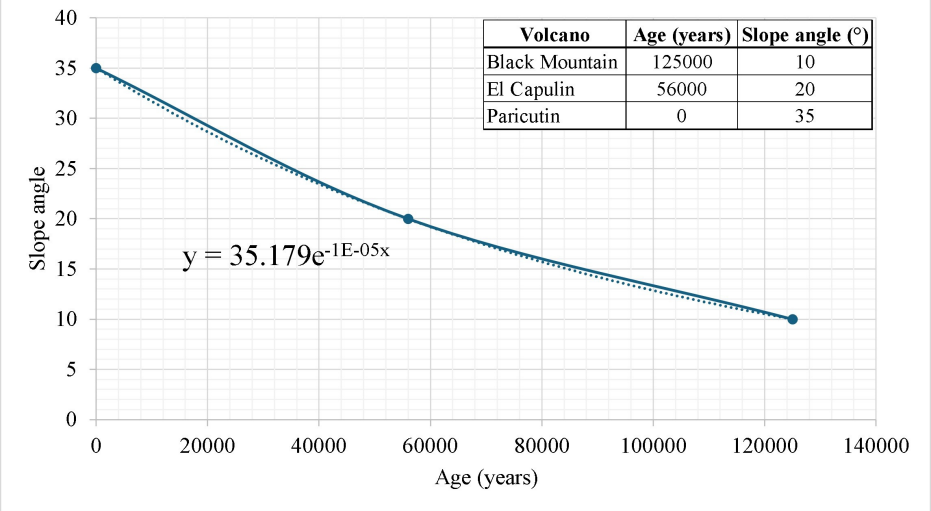

Figure 4. Exponential plot showing the correlation between slope angle and absolute dating. The trend equation was used to calculate the geomorphometric age of the cinder cones. Note the values used for the Black Mountain, Capulín, and Paricutín.

To provide an approximation of Quaternary cinder cone ages, the variable X must be solved, which represents the age in Equation (3), where Y is the slope angle. The ages were calculated for each cone in Microsoft Excel.

4. Results

The cinder cones' geomorphometric analyses from CVF show slope angles ranging from 3˚ to 13˚ and calculated ages ranging from 226,671 to 99,408 years (Table 2).

Table 2. Geomorphometric measurements and age calculations for the CVF cinder cones.

Cinder cone	Lat. (UTM)	Long. (UTM)	Base elevation (avg)*	Maximum cone elevation (avg)*	Cone height (h)*	Radio	Slope Angle (˚)	Age (years)
CC01	3049281	540731	1695.02	1723.29	28.269	247.7	6.5	168,414.57
CC02	3,065,593	541,138	1639.72	1700.34	60.625	269.5	12.6˚	102,225.11
CC03	3,061,581	541,535	1643.83	1695.07	51.24	492.92	5.9˚	178,099.55
CC04	3,060,532	545,190	1642.91	1681.61	38.699	263.31	8.35˚	143,368.63
CC05	3,055,266	546,765	1652.07	1692.65	40.579	270.17	8.5˚	141,588.17
CC06	3,052,686	549,088	1636.57	1686.56	49.984	265.17	10.6˚	119,509.39
CC07	3,066,837	542,876	1625.97	1680.00	54.024	361.08	8.5˚	141,588.17
CC08	3,060,135	552,693	1602.42	1652.59	50.169	350.17	8.15˚	145,793.00
CC09	3,052,151	554,365	1515.73	1539.36	23.637	325.83	4.13˚	213,767.05
CC10	3,063,152	552,774	1531.716	1570.73	38.512	313	7˚	161,003.77
CC11	3,055,532	555,222	1548.36	1578.64	30.288	303.33	5.7˚	181,548.17
CC12	3,065,049	556,683	1548.51	1595.14	46.632	267.35	9.88˚	126,543.54
CC13	3,052,664	559,128	1544.85	1582.15	36.888	292	7.18˚	158,464.85
CC14	3,056,319	560,341	1549.75	1572.07	22.32	294.75	4.32˚	209,269.25
CC15	3,053,748	563,389	1518.35	1541.67	23.326	366.42	3.63˚	226,671.52
CC16	3,071,450	555,525	1452.44	1488.02	35.58	316.17	6.42˚	169,652.98
CC17	3,066,342	559,191	1541.83	1593.36	51.537	373.42	7.85˚	149,543.43
CC18	3,067,623	563,945	1612.59	1648.86	36.263	325.58	6.35˚	170,749.31
CC19	3,066,740	564,974	1610.71	1643.27	33.646	378.58	5˚	194,651.00
CC20	3,065,952	573,456	1580.54	1600.51	19.9725	211.08	5.4˚	186,954.89
CC21	3,065,605	575,105	1552.96	1629.64	76.68	366.08	11.82˚	108,615.49
CC22	3,063,857	582,526	1534.72	1576.70	41.976	238.18	9.98˚	125,536.48
CC23	3,062,298	584,695	1497.13	1519.54	22.416	305.08	4.2˚	212,086.34
CC24	3,071,841	572,956	1623.74	1662.99	39.249	336.42	6.65˚	166,133.10
CC25	3,073,255	569,061	1669.80	1726.07	56.266	269.08	11.8˚	108,784.84

Continued

CC26	3,075,493	566,967	1649.35	1675.34	25.995	274	5.42˚	186,585.21
CC27	3,078,401	567,353	1763.70	1805.63	41.937	278	8.57˚	140,768.01
CC28	3,079,164	567,439	1771.92	1852.56	80.634	397.58	11.45˚	111,795.82
CC29	3,075,401	569,569	1708.11	1766.76	58.65	354.42	9.38˚	131,736.81
CC30	3,072,733	573,696	1629.18	1662.65	33.469	342.67	5.57˚	183855.2828
CC31	3,071,858	578,761	1612.07	1673.66	61.59	487.08	7.2˚	158,186.69
CC32	3,074,213	576,896	1627.21	1669.97	42.769	352.17	6.92˚	162,153.21
CC33	3,076,282	575,033	1689.57	1789.71	100.141	448.42	12.58˚	102,383.96
CC34	3,080,532	572,203	1720.83	1787.90	67.07	386.83	9.8˚	127,356.55
CC35	3,081,678	567,997	1770.46	1826.24	55.781	248.69	12.6˚	102,225.11
CC36	3,082,877	566,992	1770.76	1799.48	28.721	265.08	6.18˚	173,462.96
CC37	3,081,814	564,679	1785.51	1851.67	82.711	414	8.16˚	145,670.37
CC38	3,081,814	564,679	1722.73	1755.35	32.626	288.92	6.43˚	169,497.33
CC39	3,084,631	567,150	1756.75	1868.98	112.237	487.33	12.96˚	99,408.02
CC40	3,084,462	565,862	1818.12	1866.99	48.872	310.5	8.93˚	136,653.15
CC41	3,084,845	564,439	1581.93	1680.04	98.113	429.5	12.86˚	100,182.62
CC42	3,086,596	561,133	1503.16	1559.15	55.997	353.25	9˚	135,872.33
CC43	3,088,150	559,374	1397.12	1438.10	40.9755	291.92	8˚	147,650.63
CC44	3,089,873	545,048	1682.46	1742.41	59.946	306.5	11˚	115,805.26
CC45	3,088,777	565,274	1775.39	1834.00	58.604	364.08	9.13˚	134,438.22
CC46	3,085,348	569,021	1595.30	1643.30	47.998	373.42	7.32˚	156,533.76
CC47	3,054,677	552,039	1756.79	1810.22	53.429	268.25	11.25˚	113,557.98
CC48	3,087,155	569,779	1728.31	1797.95	69.634	417.92	9.45˚	130,993.31
CC49	3,088,569	570,215	1685.16	1751.40	66.242	418.67	9˚	135,872.33
CC50	3,093,824	563,696	1630.02	1688.47	58.45	409.67	8.11˚	146,285.00
CC51	3096940	550922	1392.49567	1438.3485	45.853	162.71	8	147,650.63

*All distances are in meters.

Since the cone age is related to the slope angle, the volcanoes analyzed can be clustered in three groups: 1) the oldest ones (3.6˚ - 6.9˚) with ages ranging from 226,671 to 162,153 years; 2) the intermediate age cones (7˚ - 9.98˚), with ages from 161,003 to 125,536 years; and 3) the youngest ones (10.6˚ - 12.96˚), with ages from 115,805 to 99,408 years (see **Figure 5**).

When analyzing the slope angles versus their corresponding geomorphometric ages, the data did not form a continuous gradient (**Figure 4**). This division into three age classes is supported by the natural clustering observed in the histogram of slope-angle frequency relationships (**Figure 5**). Having fewer or more than

three classes would introduce artificial subdivisions not supported by the data distribution and would reduce the robustness of each group by producing clusters with very small sample sizes.

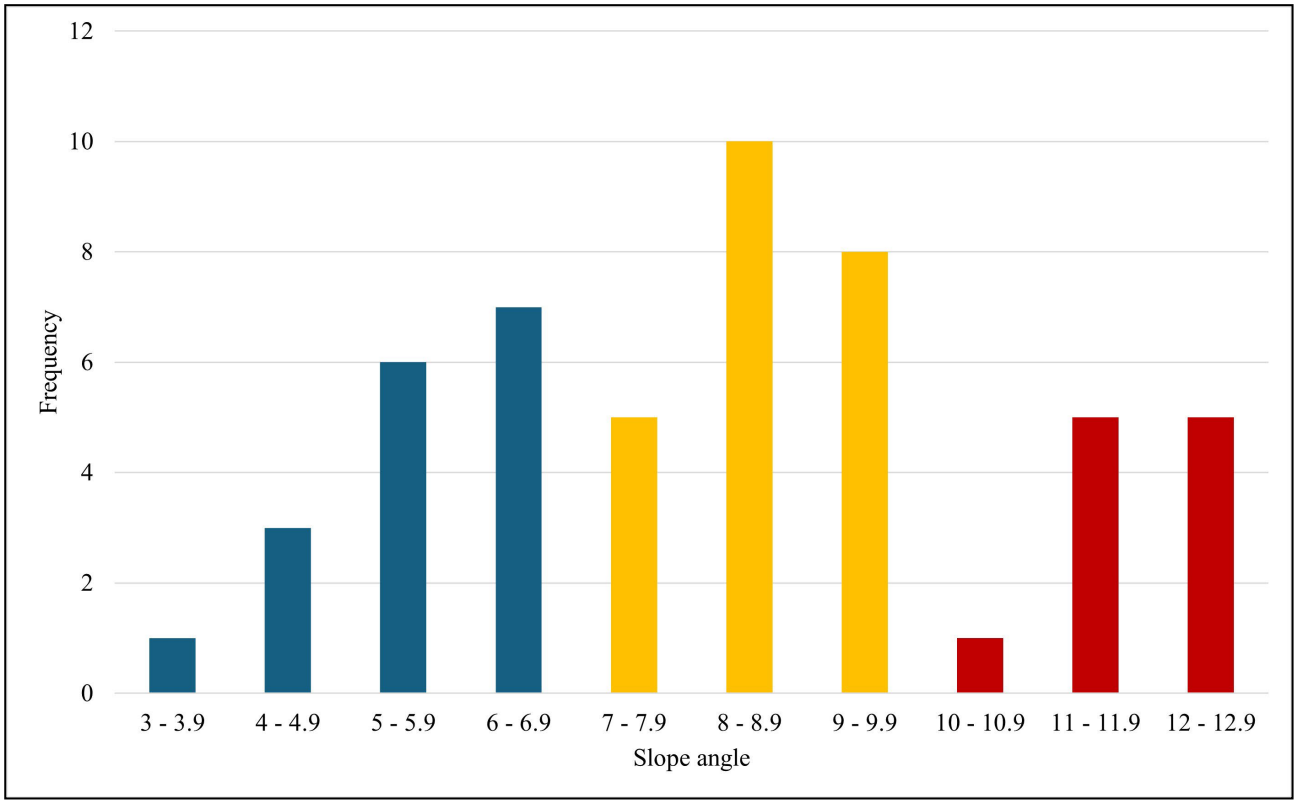

Figure 5. Histogram of cinder cone slope angle frequency in CVF. Colors indicate the three age groups: blue is the oldest, yellow is the intermediate, and red is the youngest.

To validate the slope angles calculated from remote sensing measurements, one of the cinder cones (CC51) was measured in situ. For this cone, the calculated slope angle was 8˚, and on the field, using a Brunton compass, the angle was 8.7˚. Since this small difference (0.7˚) may be due to several factors, such as the scale of measurement, instrument precision, etc., it is necessary to calculate the slope angle using survey instrumentation to obtain more precise data.

For the northernmost cinder cones of CVF, remote sensing analyses included Google Earth and drone images. The results are presented in **Table 3**. Just two cones were analyzed using drone imagery because access to this area is restricted and the land is privately owned. However, these two cones, being next to the road, allowed them to be measured without risking the drone or the handlers.

The digital elevation models (DEMs) and Google Earth images yield similar results, whereas the drone images, in both cones, indicate an age approximately 40,000 years younger.

Radiometric dating of 5 sites within the CVF (12) shows that the oldest lavas outcrop in the SW part of the volcanic field and become younger toward the NE (see **Figure 1**).

Table 3. Geomorphometric measurements and age calculations for 2 of the northernmost cinder cones in CVF, using 3 different types of images.

Cinder cone	Lat. (UTM)	Long. (UTM)	Type of image	Base elevation (avg)*	Maximum cone elevation (avg)*	Cone height (h)*	Radio*	Slope Angle (˚)	Age (years)
CC50	3,093,824	563,696	DEMs	1630	1688.5	58.5	409.67	8.11	146,285.00
			Google Earth	1370	1436	66	559.115	6.73	164,937.27
			Drone	1400	1478	78	333.657	13.15	97,952.61
CC51	3,096,940	550,922	DEMs	1392.50	1438.30	45.9	162.71	8.00	147,650.63
			Google Earth	1432	1537	105	715.667	8.35	143,368.63
			Drone	1420	1510	90	427.1	11.90	107,940.95

*All distances are in meters.

5. Conclusions

Of the approximately 300 cinder cones in CVF, only 51 could be measured using remote sensing techniques, including DEMs, Google Earth, and drone images. Only a sixth part of the cones have a preserved shape that allowed them to be measured.

The geomorphometric ages were calculated using an exponential trend that correlates radiometric ages with slope angles for 3 known cinder cones from arid zones. The trend expressed an equation that permitted the calculation of the age of a cinder cone under those climatic conditions. The ages of the 51 cinder cones range from 226,671 to 99,408 years, based on DEMs and Google Earth images. The cinder cones were arranged into 3 groups: the oldest to the SW part of the volcanic field, the intermediate-age in the central part of the field, and the younger ones in the north-northeastern portion of the CVF. It coincides with the evolution of CVF, explained by previous work [12]. Therefore, the three-class classification represents the most coherent and geologically meaningful partition of the dataset, capturing the main phases of cone degradation and providing a consistent framework for comparative analysis.

The drone images of two of the northern cones, close to the site and radiometrically dated to 0.09 Ma, yield an age of 97,952 years, while the other images yield ages of 146,000 to 164,000 years. Since the drone captured images with a spatial resolution of 9.47 cm, it can be inferred that errors are lower and calculations are more accurate; however, future work should focus on acquiring additional high-resolution drone data to validate this finding across the entire volcanic field.

Geomorphometric dating can provide an initial idea of a cinder cone's age in arid zones, but it is not a definitive age. It is recommended as a tool for obtaining preliminary dates within a young basaltic volcanic field, but absolute/radiometric dating remains the better option for reconstructing the volcanic activity history of the area.

Acknowledgements

The authors gratefully acknowledge the contributions of all project members: our students (*Martha Gallegos, Esmeralda Chavez, Ricardo Contreras & Irlanda Ramos*) and drone specialists (*Aracely Lopez & Fabricio Madrigal*) for all their effort and for rigorous data acquisition, analytical support, and constructive discussions throughout the development of this long-term project. Their commitment to methodological precision and continuous feedback significantly strengthened the quality and scope of the study submitted here.

Conflicts of Interest

The authors declare no conflicts of interest regarding the publication of this paper.

References

[1] Balaram, V. (2020) Current and Emerging Analytical Techniques for Geochemical and Geochronological Studies. *Geological Journal*, **56**, 2300-2359. https://doi.org/10.1002/gj.4005

[2] Dickin, A.P. (2018) Radiogenic Isotope Geology. Cambridge University Press. https://doi.org/10.1017/9781316163009

[3] Gradstein, F.M. and Ogg, J.G. (2020) The Chronostratigraphic Scale. In: *Geologic Time Scale* 2020, Elsevier, 21-32. https://doi.org/10.1016/b978-0-12-824360-2.00002-4

[4] Faure, G. and Mensing, T.M. (2007) Earth: Model of Planetary Evolution. In: Faure, G. and Mensing, T.M., Eds., *Introduction to Planetary Science*: *The Geological Perspective. Earth*: *Model of Planetary Evolution*, Springer, 65-86. https://doi.org/10.1007/978-1-4020-5544-7_6

[5] Pike, R.J., Evans, I.S. and Hengl, T. (2009) Chapter 1. Geomorphometry: A Brief Guide. In: *Developments in Soil Science*, Elsevier, 3-30. https://doi.org/10.1016/s0166-2481(08)00001-9

[6] Pelletier, J.D. and Cline, M.L. (2007) Nonlinear Slope-Dependent Sediment Transport in Cinder Cone Evolution. *Geology*, **35**, 1067-1070. https://doi.org/10.1130/g23992a.1

[7] Miller, J.G. (2006) A Morphologic Analysis of Quaternary Cinder Cones, Potrillo Volcanic Field, New Mexico. Master's Thesis, University of Texas at El Paso.

[8] Chávez Armendáriz, E. (2021) Estudio geomorfométrico de dos conos cineríticos al norte del Campo Volcánico de Camargo, Chih. Bachelor's Thesis, Universidad Autónoma de Chihuahua.

[9] Gallegos-Aragón, M.I. (2013) Análisis geomorfométrico de conos cineríticos del Cuaternario en el Campo Volcánico de Camargo, Chihuahua, México. Bachelors Thesis, Universidad Autónoma de Chihuahua.

[10] Noyola-Medrano, M.C. (1995) Estudio comparativo de la geología y morfología de algunos conos cineríticos en los campos volcánicos de Camargo, Chih. y San Quintín, BC. Bachelors Thesis, Universidad Autónoma de San Luis Potosí.

[11] Scott, D.H. and Trask, N.J. (1971) Geology of the Lunar Crater Volcanic Field, Nye County, Nevada.

[12] Aranda-Gómez, J.J., Luhr, J.F., Housh, T.B., Connor, C.B., Becker, T. and Henry, C.D. (2003) Synextensional Pliocene-Pleistocene Eruptive Activity in the Camargo Vol-

canic Field, Chihuahua, México. *Geological Society of America Bulletin*, **115**, 298-313. https://doi.org/10.1130/0016-7606(2003)115<0298:sppeai>2.0.co;2

[13] Cameron, K.L., Robinson, J.V., Niemeyer, S., Nimz, G.J., Kuentz, D.C., Harmon, R.S., *et al.* (1992) Contrasting Styles of Pre-Cenozoic and Mid-Tertiary Crustal Evolution in Northern Mexico: Evidence from Deep Crustal Xenoliths from La Olivina. *Journal of Geophysical Research*: *Solid Earth*, **97**, 17353-17376. https://doi.org/10.1029/92jb01493

[14] Royo-Ochoa, M., Alva-Valdivia, L.M., Fucugauchi, J.U., Chavez-Aguirre, R., Goguitchaichvili, A., Solé, J., *et al.* (2004) Magnetic Polarity Stratigraphy and K-Ar Dating in the Camargo Volcanic Field, Northern Mexico: Lateral SW-NE Migration of Volcanic Activity. *International Geology Review*, **46**, 558-573. https://doi.org/10.2747/0020-6814.46.6.558

[15] Aranda-Gómez, J.J., Housh, T.B., Luhr, J.F., Noyola-Medrano, C. and Rojas-Beltrán, M.A. (2010) Origin and Formation of Neck in a Basin Landform: Examples from the Camargo Volcanic Field, Chihuahua (México). *Journal of Volcanology and Geothermal Research*, **197**, 123-132. https://doi.org/10.1016/j.jvolgeores.2009.08.004

[16] Wood, C.A. (1980) Morphometric Analysis of Cinder Cone Degradation. *Journal of Volcanology and Geothermal Research*, **8**, 137-160. https://doi.org/10.1016/0377-0273(80)90101-8

[17] Bloomfield, K. (1975) A Late-Quaternary Monogenetic Volcano Field in Central Mexico. *Geologische Rundschau*, **64**, 476-497. https://doi.org/10.1007/bf01820679

[18] Gilichinsky, M., Melnikov, D., Melekestsev, I., Zaretskaya, N. and Inbar, M. (2010) Morphometric Measurements of Cinder Cones from Digital Elevation Models of Tolbachik Volcanic Field, Central Kamchatka. *Canadian Journal of Remote Sensing*, **36**, 287-300. https://doi.org/10.5589/m10-049

[19] Kereszturi, G., Geyer, A., Martí, J., Németh, K. and Dóniz-Páez, F.J. (2013) Evaluation of Morphometry-Based Dating of Monogenetic Volcanoes—A Case Study from Bandas Del Sur, Tenerife (Canary Islands). *Bulletin of Volcanology*, **75**, 1-19. https://doi.org/10.1007/s00445-013-0734-1

[20] Porter, S.C. (1972) Distribution, Morphology, and Size Frequency of Cinder Cones on Mauna Kea Volcano, Hawaii. *Geological Society of America Bulletin*, **83**, 3607-3612. https://doi.org/10.1130/0016-7606(1972)83[3607:dmasfo]2.0.co;2

[21] Zarazúa-Carbajal, M.C. and De la Cruz-Reyna, S. (2021) Digital Elevation Model Resolution: Effects on the Chronometry-Oriented Morphological Analysis of Monogenetic Scoria Cones in the Sierra Chichinautzin, Central Mexico. *Geomorphology*, **389**, Article ID: 107842. https://doi.org/10.1016/j.geomorph.2021.107842

[22] Foshag, W.F., Gonzalez, J.R., McKay Douglas and Wrather, W.E. (1956) Birth and Development of Paricutin Volcano Mexico: Geologic Investigations in the Paricutin Area.

[23] Anthony, E.Y. and Poths, J. (1992) ^{3}He Surface Exposure Dating and Its Implications for Magma Evolution in the Potrillo Volcanic Field, Rio Grande Rift, New Mexico, USA. *Geochimica et Cosmochimica Acta*, **56**, 4105-4108. https://doi.org/10.1016/0016-7037(92)90022-b

[24] Stroud, J.R. (1997) The Geochronology of the Raton-Clayton Volcanic Field, with Implications for Volcanic History and Landscape Evolution. MSc, New Mexico Institute of Mining and Technology.